TWELTH EUROPEAN ROTORCRAFT FORUM

Paper No. 17

MEASUREMENT OF SIDE FORCES OF A H-FORCE ROTOR

Henry R. Velkoff*
Christian Petersilge
Curtis Cowan

The Ohio State University
Columbus, Ohio, USA

*Presently U.S. Army ARTA, AVSCOM
Ames Research Center
Moffett Field, California

September 22 - 25, 1986

Garmisch-Partenkirchen
Federal Republic of Germany

Deutsche Gesellschaft fur Luft- und Raumfahrt e. V. (DGLR)
Godesberger Allee 70, D-5300 Bonn 2, F.R.G.

MEASUREMENT OF SIDE FORCES OF A H-FORCE ROTOR

ABSTRACT

As was reported in the Seventh European Forum, study of the use of tip vanes has been underway to investigate both the impact of the vanes on hover performance and on their potential use as force generators. It is the aim of this paper to report on progress made to determine the forces that can be generated. Model tests were run using a six foot diameter rotor with tip vanes pivoted below the blade tips. Data were taken on the thrust, torque, and side-force. The results obtained were in substantial agreement with the side force predicted by using a simple wing model.

BACKGROUND

The primary motivation for utilizing vanes at the tips of helicopter rotor blades is to provide a force in the plane of rotor which is independent of the tilt of the lift vector. A force so obtained could be used in two separate ways. It could be used as a propulsive force and so act as a propeller would in a compound helicopter. Coupled with an added small wing, higher flight speeds could be achieved but with less complexity than the propeller and its associated drive system.

The second use for the force would be to provide the pilot with an independent control force which would be of use at low flight speeds. It would allow for more precision positioning in hover as well as for added maneuvering such as lateral translation in N.O.E. flight.

Previous analytical studies have indicated the potential gains as a propulsor and have been directed at the effect of the vanes upon hover performance (1). Analysis showed that a significant gain in speed was possible. From tests it was also found that the vanes, if properly located, would not adversely affect hover performance. In some tests it was found that the vanes actually increased performance (2). Such a gain was not consistently repeatable, however (3).

The arrangement of the vanes at the tips that has evolved is shown in Figure 1. There it can be seen that the vanes are located below the tip. The vanes are pivoted about an axis that is perpendicular to the chord plane of the airfoil. The motion of the vanes is depicted in Figure 2. The action is similar to that used in the rotating vane propulsors used in some German tug boats (4).

EXPERIMENTAL PROGRAM

No test data were available on the forces that can actually be developed by tip vanes in the configuration shown. Consequently a test of a model rotor equipped with tip vanes ws undertaken. An 80-inch (2.03 m), three bladed rotor was fabricated with tip vanes located below the blade tips. The rotor had a blade chord of 6.125 inches (.156 m), a vane chord of 6.125 inches (.156 m) with a vane span of 6 inches (1.152 m). The model was mounted on a hover stand with the plane of rotation at ten feet (3.05 m) above the floor. Two 8 horsepower

(5.97 KW), air motors were used to drive the rotor. Tests were run at with selected values of blade pitch angle, blade vane angle and rotor speed. Initially measurements were taken of the thrust, torque, rotor speed, and side forces in two planes.

Design of H-Force Airfoil and Hub

Previous tests conducted by Velkoff and Parker (2), which compared various tip vane configurations, indicated that a single downward tip vane attached to the end of each blade might increase the performance of the rotor. High centrifugal forces at the blade tips presented an obvious constraint to the weight and strength of the tip vane and its attachment. The use of T tips was considered to reduce the bending moment and create symmetric loading about the blade axis, but the possibility of achieving increased performance while creating a side force led to the use of the downward tip vanes.

The primary airfoil used the blades as well as for the tip vane was a NACA 0016. In order to provide for a seal between vane and blade surface, the symmetric shape of the blades was altered by flattening the bottom of tips. This provided a smooth surface for the tip vane to oscillate against. A smooth transition was achieved between the NACA 0016 and the "Clark Y" flat bottomed blade tip. The "Clark Y" was formed to be 16-percent thick. Figure 3 illustrates the blade configuration.

The motion of the tip vanes was controlled by an eccentric cam located in the center of the hub. The amount of tip vane motion was adjustable, but had to be fixed during operation. The push rods for the tips were enclosed in the blades and were positioned aft of the quarter chord. This allowed the blade angle to be fully adjustable without affecting the push rod movements since blade pitch adjustment also took place at the same chord.

Blade and Tip Vane Design

The rotor blades are made of four sections of poplar wood each running the entire length of the blade. The seam between these pieces is strengthened with a wooden spline and a steel strap. The high centrifugal loads of the tip are carried by the steel strap. A "U" shaped clevis fits flush over the tip end of the blade and resists the outward moment generated by the tip vane. Centrifugal forces of the tip vane are also transmitted through this clevis to the steel strap.

At the root end of the blade another clevis attaches the blade to the hub. These clevi were specially fitted to each blade to ensure proper alignment of the tip vane push rod which passes through the clevis and the wall of the hub. The inboard portion of the clevis is a threaded 3/4" spindle used to firmly attach the blade to the hub. The push rod passes through the center axis of this spindle.

The weight of the tip vanes was reduced by making the front section from solid balsa wood. The tail section was made of a balsa wood rib structure covered with a 1/32" balsa skin. A layer of epoxy resin and fiberblas cloth was added to make it stronger and more durable. The rotation of the tip vanes about their quarter chord was achieved using a steel pin with two bearings

housed in a steel sleeve. The sleeve was epoxied into the solid balsa section of the tip. The spindle pin protruded out of the tip vane, so that it could be attached to the clevis located on the blade tip. Another pin located 0.8 in (2.03 cm) of an inch aft of the quarter chord was used to transmit motion from the push rods to the tip vane. The connection of the push rod to the pin was made with a spherical bearing rod end located in a recess at the tip of the main blade.

The tip vanes were balanced chordwise about their rotating pins to reduce the centrifugal loads in the push rods and cam mechanisms. The chordwise center of gravity of each tip was shifted to within a few hundredths of an inch aft of the quarter chord. This balancing technique created an effective 32 grams of tensile force per g of tip acceleration. At full speed operation, this resulted in a 35 pound load. The push rods were made of hollow steel tubes to further reduce centrifugal loading on the root fittings. At each end of the rods a solid threaded section was welded in place. The rod ends at the tip end had left handed threads and those in the hub had right handed threads. The combination of right and left handed threads allowed the rod to be used like a turn buckle. This proivded an adjustment method for the zero position of the tip vanes.

Design of Hub and Cam Mechanism

The mount between each of the blades and the hub was rigid, but allowed rotation of the blades about their quarter chord. This simplified the linkage mechanism between the cam and the push rods. This meant that the rotor was rigid and in plane and fixed relative to the shaft. The hub itself is bowl shaped with the cam operating in the center. The hub is made of an aluminum cylinder that has 3/4 of an inch thick walls with a 9 inch outer diameter and 3 inches high. The cylinder has three equally spaced mounting positions for the blades. The bottom of the cylinder is attached to a steel plate that is fastened to the drive shaft.

In the center of the hub is an eccentric cam. The cam drives the push rods that control the tip vane movement. The zero azimuth of the tip motion is held fixed to the ground reference by means of an overhead boom and a rubber hose that prevents the eccentric center of the cam from rotating with the blades. The cam is made of two solid cylinders that are held from rotation by the hose. One cylinder is mounted inside the other but they are not mounted concentrically. The eccentricity of the cam is adjusted by rotating the cylinders and locking them into place with set screws. A bearing is mounted in a ring that surrounds the cam and follows the eccentric motion. Three actuation pins mounted on the ring move in a circular fashion. The torque to drive the cam and the push rods comes form the drive shaft. Figure 4 shows how the motion is converted from eccentric circular motion to the linear motion of the push rods using the slider pin cam follower. The pin is mounted on the eccentric portion of the cam. A small roller bearing separates it from the slotted slider cam follower. As the pin moves in a circular path within the rotating hub, it drives the push rod radially.

Three rubber straps are used between the central drive shaft and the hub to allow the ring to move eccentrically while maintaining azimuthal position. The eccentric motion of the ring provides the circular motion to the pins as shown in Figure 4. The resulting motion of the tips, if plotted against azimuth position, would look nearly sinusoidal. A study of the motion generated during a static test of a prototype for this cam showed that actual motion differed by only a few percent from the pure sinusoidal motion (5).

Test Stand and Instrumentation

The entire measurement system has been automated to reduce the work load of the operator during the test. All data is measured and sent directly to the computer for storage. The operator is needed only to control the rotational speed and operate an on-site remote computer terminal. Data is displayed on the terminal virtually instanteously.

Mechanical System

The mechanical portion of the instrumentation system includes the test stand which support and powers the rotor, as well as the fluxures used to isolate the forces for individual measurement. Rotor speed was measured by means of a magnetic pickup sensing a 56 toothed gear and a digital counter.

The test stand is comprised of a fixed base structure and a mast. The rotor mast is supported to the base by flexures. The mast which houses a 7 foot drive shaft is suspended inside and above the fixed base of the test stand. The base of the test stand is a welded steel frame firmly bolted to the floor. Two drive motors are mounted directly to the base. Power is transmitted to the drive shaft by means of two opposing belt and pully systems. Driving torque is measured by a strain gage flexure. The electrical signals are passed through a set of slip rings to the stationary system. The torque flexure has been used in earlier testing and was recalibrated for these tests.

The mast and drive shaft were mounted to the base with steel flexures and with a rubber diaphram. This mechanism allowed vertical deflection and pivoting about the rubber plate. The resulting motion was similar to that of a ball joint whose pivot could also move vertically. Figure 5 shows the H-force flexures.

Thrust was measured with two strain gage flexures mounted just below the rubber plate. Deflections at this point are primarily vertical. Side forces were measured with steel flexures attached to the mast 23 inches above the rubber pivot plate. At this point the freedom of movement is primarily horizontal in both x and y directions with very slight vertical translation associated with thrust changes. The side force flexures are mounted at 90 degree intervals around the shaft. Each has a vertical and a horizontal flexure connected toform an upside down L shaped leg. The horizontal section is connected to spring steel flexures which are also attached to the mast. The combination of vertical, horizontal, and spring steel flexures separate the x, y, and z movements of the mast. The arrangement is shown in Figure 6. Each of the four horizontal forces are measured in the four vertical flexures. Two of them are x direction sensitive, and the other two are y direction sensitive. The strain gages used to measure side forces are mounted near the base where the larger bending moments give greater sensitivity. The spring steel members allow the mast to move in both the x, and y directions without being restricted by the stiff axis of the other flexures.

VIBRATION

The natural frequency of the mast and rotor was observed to be 4 Hz. System damping was very small. It was necessary to accelerate and decelerate through the natural frequency as rapidly as possible. The rotor was balanced

using a Production Measurement Corporation Model 206 vibration analyzer. The resulting amplitude of vibration was 2 to 5 thousands of an inch depending on the testing configuration. The amplitude of vibration was monitored through out the testing procedure with the vibration analyzer. When large vibration was observed, the rotor was rebalanced using the vibration analyzer. Much of the fluctuation in the side force channels was due to inbalance and shaft whirl creating periodic fluctuations of constant amplitude.

Measurement System

The electrical portion of the measurement systrem consists of the strain gage elements, carrier amplifiers, operational dc amplifiers, and an analog to digital interface. Six measurements were made using strain gage flexures. These include torque, thrust, and four side force measurements. The side forces measured were planer, requiring only two measured components; the other two side force measurements were redundant and provided a means for checking results.

The H-force flexures are used to restrain the lateral movement of the mast relative to the base. There are four strain gages mounted on each of the flexures. Figure 6 depicts a schematic of the electrical system. The bridge circuit is shown is used on all measurement flexures. Only the torque channel required slip rings to pass electrical signals fromt the rotating shaft. The four side force and thrust measurements are wired directly to the carrier amplifiers. The strain gages used are type ED-DY-100BR-350 made by Micro Measurements. They are steel compensated with a gage factor of 3.17. The bridge measured only the bending component of stress.

Each of the six measurement channels require a carrier amplifier circuit to provide an excitation voltage and to detect the change in output voltage. Two carrier amplifiers, a Consolidated Engineering Corporation Type 1-118 carrier amplifier and a Consolidated Electrodynamics Corporation Type 1-127 were used. Another set of amplifiers was designed to adapt the low output voltage to the required +/- 16 volt scale of an A/D converter.

Sampling and Averaging Technique

Data was interfaced to the computer directly through the A/D converter. As mentioned earlier, the A/D could sample only 3 channels. The switching was done manually by the operator. A General Terminal Corporation type GT-100 terminal was used in the lab to display data and direct the operator when to switch active channels. Sampling of each of the three active channels was done simultaneously. The sampling rate was set by the rotor speed so that data was taken every degree of revolution. The buffer of the A/D required that 4096 data points be taken for each channel. A subroutine was used to average only the first 3600 data points. The result was a time averaged signal for exactly 10 revolutions.

The time averaging feature whch the computer provided was a very important part of the measurement system. Because of signal fluctuation averaging was necessary. Sampling was done for exactly 10 revolutions to reduce the biasing of the measurement. Some biasing could have occurred due to the beat frequency which was several times slower than the rotating frequency.

Interactive Procedure

During the test, only the blade angle and the speed were entered by the operator. All other measurements were made with the A/D link as previously mentioned. The frequency counter used to measure the speed was a Simpson model 710.

The rotor operation was steady under all conditions tested. Previous testing of an H-force rotor with a single blade had indicated unusually high performance with dramatic changes in thrust and torque. No such large changes were observed. The speed was always allowed to settle to a steady state before measurement data were taken.

Calibration

Each of the six measurement channels were calibrated with known weights. Calibration data were taken using the same computer link methods as those used for actual measurements. Two programs were used to find and check the sensitivity of each channel.

The first program recorded the voltage equivalent outputs of each of the measurement channels, while a known load was applied in one of the primary coordinate directions. This program also calculated a linear least squares curve fit for the primary measurement and each of the secondary measurements. Ideally, there wuld be no sensitivity in the secondary channels; but unfortunately the attempt to isolate each axis of measurement was not perfect and some "crosstalk" between channels was observed. The calibration data was graphed, and linear trends were observed for both primary and secondary sensitivities.

A second calibration program was used to check the results of the first. This program used the linear least squares sensitivities found by the previous program to calculate the effective forces. This program was also interactive and displayed these results on the laboratory terminal during the calibration procedure. This proved to be a very advantageous feature, and allowed calibration checks of not only each independent measurement channel, but also combined loading conditions of thrust and side force that simulated actual running conditions.

The interacting effects between the thrust and side force measurements were found to be significant and had to be accounted for. A matrix of the interactions was set up based upon the actual calibration and was used in the data reduction.

Measurement Accuracy

The accuracy of any measurement system is a function of all possible errors affecting that system. Possible sources of measurement error included the hysteresis of the rubber diaphram and the steel flexures, zero drift of the carrier amplifiers and the voltage increasing amplifiers, and drift of amplifier gain for the carrier amplifiers and the voltage increasing amplifiers. Included are bias due to taking only 3600 data points in 10 revolutions and the beat frequency effect, and calibration errors due to cross talk and due to static sensitivity error.

The values of H-Force 1 and H-Force 2 shown here are actually average values of H1-H3 and H2-H4. The following accuracies are representative of accurcy of the data.

	Direction	Accuracy
H-Force 1	X	+/- 0.2 lbs
H-Force 2	Y	+/- 0.2 lbs
Thrust	Z	+/- 0.3 lbs
Torque		+/- 4%
Speed		+/- 1 count

It should be noted that these calibration measurements were made with no rotation.

Experimental Results

The rotor was tested with tip vane angles of +/- 0, 3, 6, 9, 12 degrees. Each of these tip angles were tested with blade angles of 0, 3, 6, 9, 12 degrees. Data were taken for all of these cases at tip speeds of 217, 224, 232 ft/sec. Another similar set of data was taken with the tip vanes removed.

The same rotor blades were used through out the testing, and an attempt was made to maintain equal testing conditions for each of the tests. Changes in air density were accounted for. Atmospheric pressure and wet and dry-bulb temperatures were used to find the air density from a psychrometric chart. Typical Reynolds numbers at the tips were from 6.86×10^5 to 7.51×10^5.

Results

The magnitude of the side force generated is shown in Figure 7. These data show the increase in side force generated with increasing vane angle magnitude. The data for a blade pitch angle of 3 degrees. The data for 664, 643, and 621 rpm are collapsed onto one curve at 664 rpm. Two separate sets of data were taken at each data point. The force increase with vane angle shows an almost linear increase up to the 9 degree magnitude and a fall off occurs when the 12 degree case is reached.

Figure 8 illustrates the results for several blade pitch angles using the 664 rpm data alone. It can be seen that the curve for a blade pitch of 0 degrees is quite separate from the other data. The 3, 6, and 9 degree data are well grouped except for the 9 degree case at the vane angle of 12 degrees where some stall phenomena may be occurring. These results imply that in the 3 to 9° pitch range there is little influence of blade pitch on the tip vane performance but a very significant interaction must be taking place between 0 and 3 degrees. This situation is graphically portrayed in Figure 9 where the H-force is plotted versus the blade pitch angle. Except for the zero vane angle magnitude, all other vane magnitude show a severe effect of blade pitch change from 0 to 3 degrees. Thus it appears that significant coupling is taking place.

If one now looks at the effect of vane magnitude on the thrust as shown in Figure 10, some interaction seems present but no strong trends are apparent. A slight fall-off in thrust seems to occur as the vane magnitude is increased from

zero but at higher vane values the slight fall off recovers. Torque variation with tip angle is shown on Figure 11. At the lower blade angles a gradual increase in torque occurs with increasing vane angle magnitude as one would expect. At the blade pitch of 12 degrees the jump in torque with blade pitch and vane angle is probably due to some stall phenomena.

Figure 12 presents typical figure of merit results. Data are shown for all rpm for the base line rotor with no tip vanes, vanes at 0 degrees magnitude, and for the 6 degree vane angle case. Although a significant drop in M is found when the tip vanes are added, only a small decrease occurs as the vanes are oscillated through $\pm$ 6 degrees. The large impact caused by the addition of the vanes can be seen more readily in Figure 13. There the torque coefficient, CQ is plotted against $CT^{3/2}$ for two cases: no tip vanes, and with tip vanes at $\pm$ 0 degrees. The large torque increase with the addition of tip vanes is clearly evident.

If the effective drag coefficient of the vanes is calculated using the data shown in Figure 13, it is found that for the vanes, C_D = 0.0227 (Calculations may be found in the appendix.) This value is higher than the value one would expect even at a relatively low Reynolds number. It is believed that some flow interaction and separation may be occurring at the juncture of the tip vane and the undersurface of the blade leading to an increase in drag of the vane-blade combination.

Calculations of the H-forces based upon calculated vane lift were conducted and are presented in the appendix.

Discussion

It is apparent from the data that the tip vanes can produce useful side forces. The values can be predicted to first order by simple aerodynamic wing theory as shown in the appendix. The drag of the vanes was somewhat higher than a well designed vane-blade interaction should allow. No evidence of enhanced performance was found with the configuration used for the H-force tests. The configuration, however, was markedly different than that found to be optimum (2).

The significant changes in force generation that occurred for blade pitch changes from 0 to 3 degrees was considered carefully. It is believed that the position of the vane, whether nose in or nose out, could possibly cause a change in the flow distribution near the blade tip. That is, the vortex patterns of the blade tip and tip vane could interact differently in the various vane positions. Since it was found from prior study that hover performance is exquisitively sensitive to any variations in vane configuration, such vane position changes could possibly affect the local flow significantly (2). If this occurred, then the lift distribution on the blade might not remain constant around the azimuth and a resulting steady moment could be introduced into the rotor mast supports. With the instrumentation used in these tests, no provision was made to measure moments, but only side forces. Thus with the test rig used, any moments produced could lead to pollution of the side force data.

It is believed that the side force data for the zero blade pitch case would not be significantly affected by the possible moments since little or no rotor lift is being produced and hence no significant lift induced vorticies would be expected.

Because of this concern over the possible generation of rotor moments due to tip vane motion, a complete revision of the instrumentation has been undertaken. This revision is outlined in appendix II. Only preliminary tests have been run and no results can be reported from that system at this time.

REFERENCES

1. Velkoff, H.R., and Parker, T.W., "Preliminary Study of the H-Force Rotor," presented at the "American Heliocopter Society," Oct. 22-24, 1980.

2. Velkoff, H.R., "Hover Tests of a H-Force Rotor," Seventh European Rotorcraft and Powered Lift Aircraft Forum, Paper No. 44, Sept. 8-11, 1981.

3. Velkoff, H.R., and Parker, T.W., "Effect of Tip Vanes on the Performance and Flow Field of a Rotor in Hover," presented at the 38th annual forum of the "American Helicopter Society," Anaheim, CA, May 1982.

4. Mueller, Hans F., "Recent Developments in the Design and Application of the Vertical Axis Propeller," transaction of "The Society of Navel Architects and Marine Engineers," 1955, Vol. 63.

5. Boudel, R., "Examination of Eccentric Cam Motion," a senior project report for th Department of Mechanical Engineering at the Ohio State University, Columbus, OH, 1980.

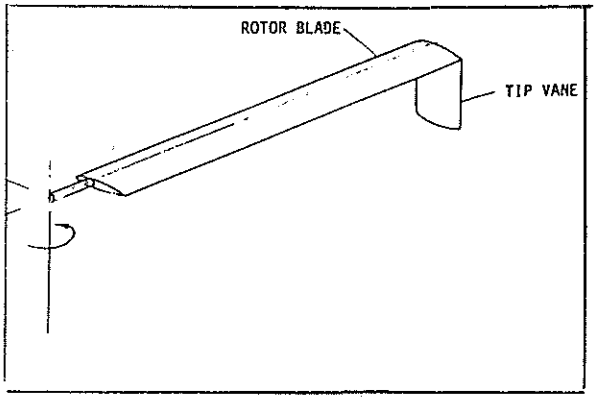

Figure 1: Rotor Blade with Tip Vane in Downward Position

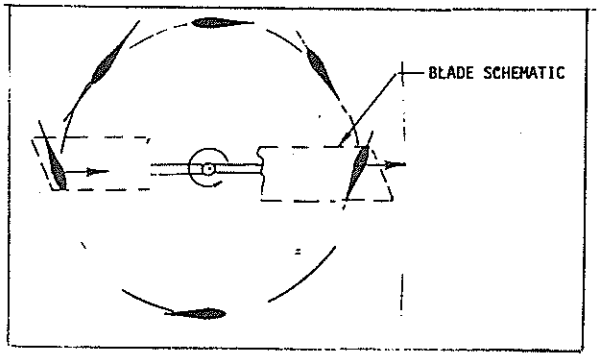

Figure 2. Tip Vane Positions While Rotating.

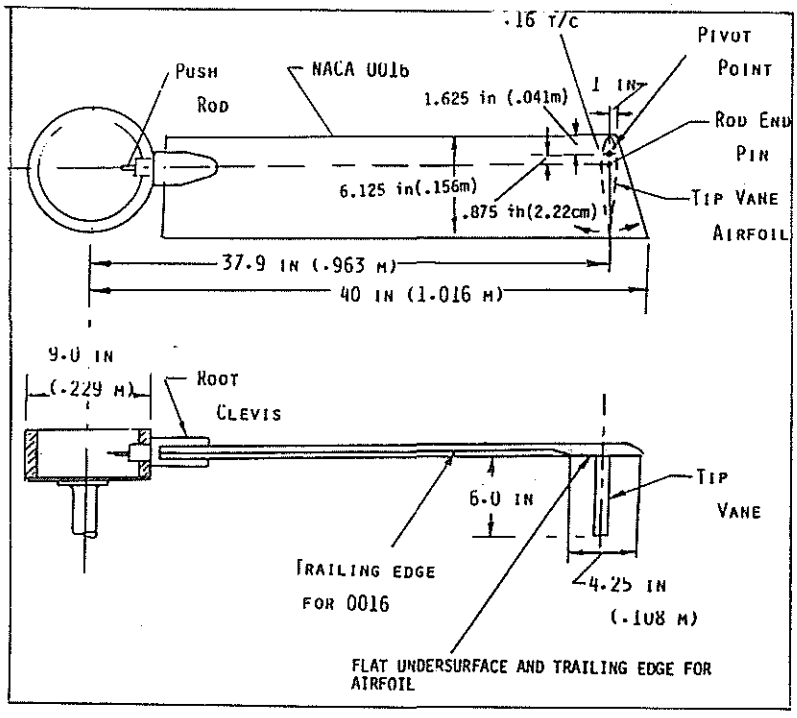

Figure 3. Blade and Tip Vane Configuration Showing the Airfoil Arrangement.

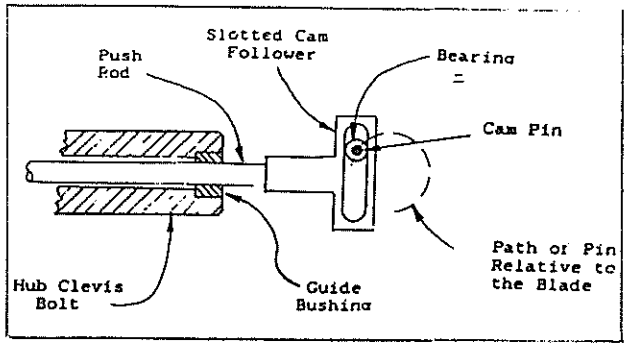

Figure 4. Slider and Pin Mechanism of Cam.

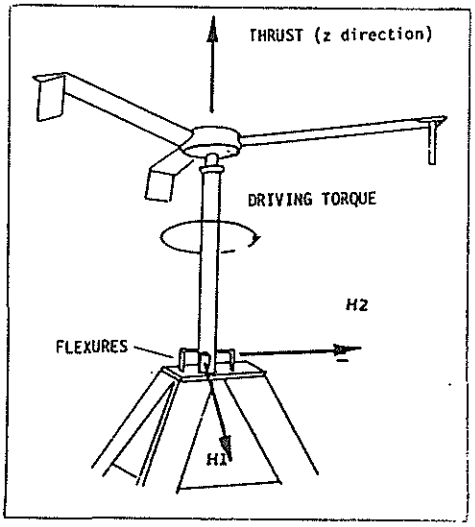

Figure 5. Coordinate System

Note the following terms:

H1 - Side force at stat. 1 (x direction)
H2 - Side force at stat. 2 (y direction)

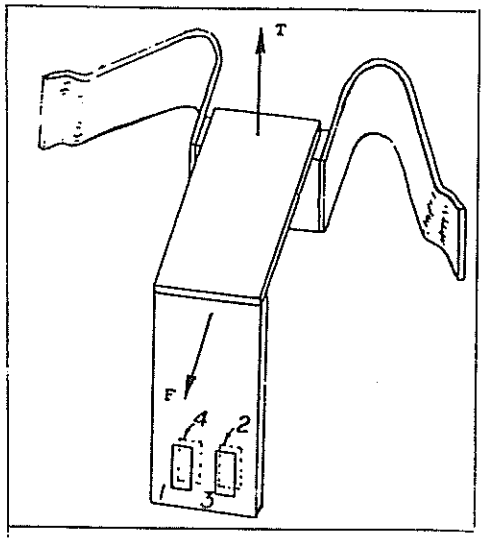

Figure 6. H-Force Flexure and Gage Locations.

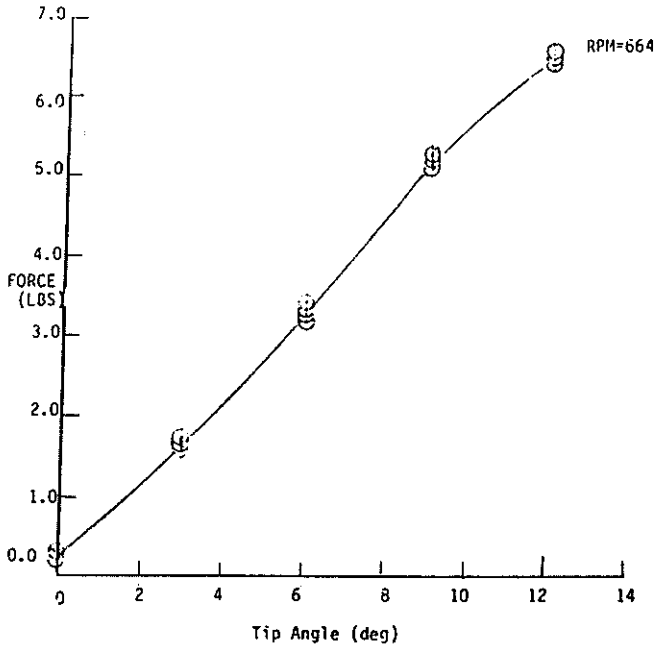

Figure 7. H-Force vs. Tip Angle
Blade Angle= 3° Constant
Hover Test of H-Force Rotor
Data Averaged Over 10 Revs
All Data Normalized to 664 RPM

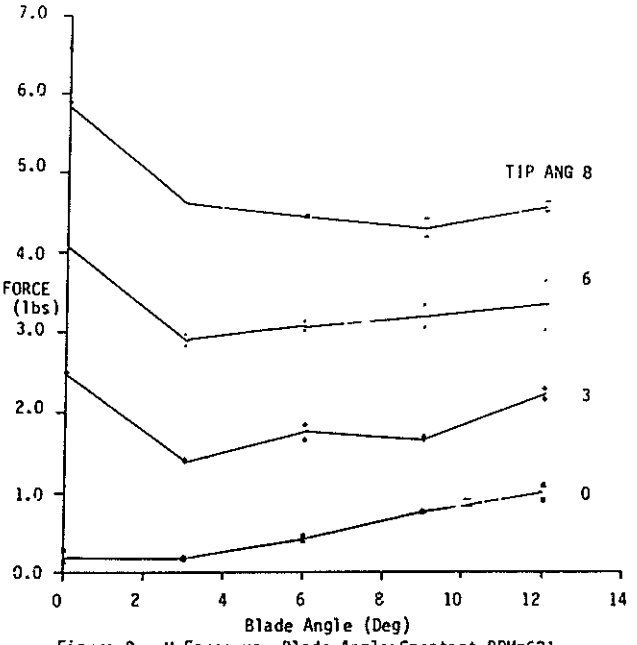

Figure 9. H-Force vs. Blade Angle: Constant RPM=621
Hover Test of H-Force Rotor
Data Averaged Over 10 Revs

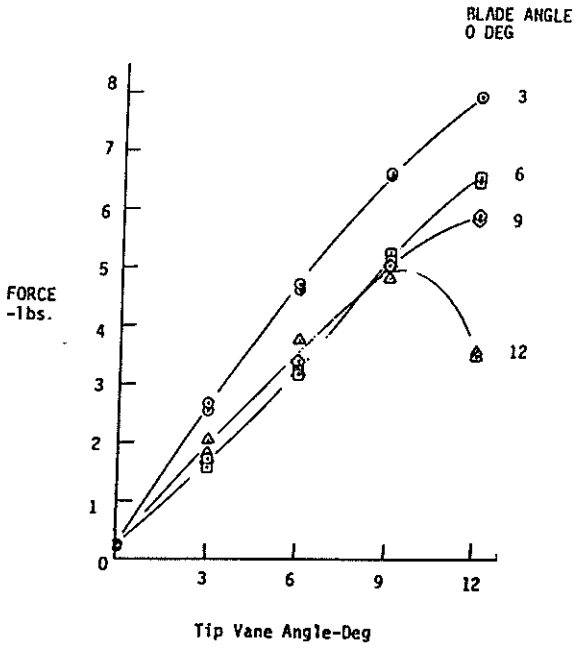

Figure 8. H-Force vs. Tip Vane Angle-664 RPM.
Data Averaged Over 18 Revs.

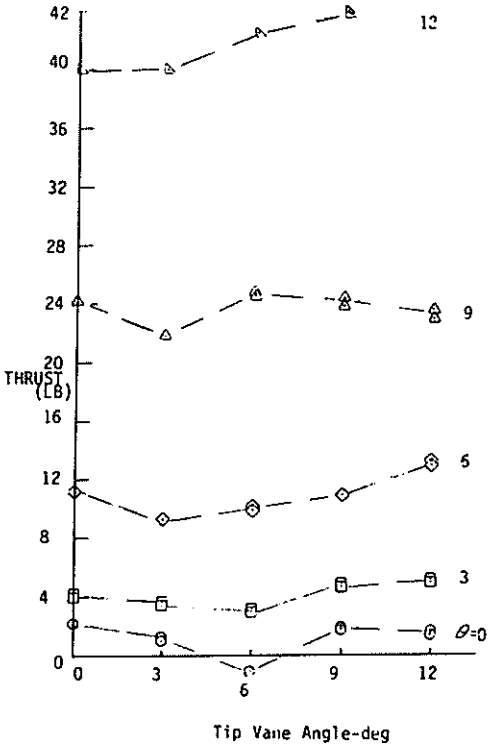

Figure 10. Rotor Thrust vs. Tip Vane Angle
664 RPM

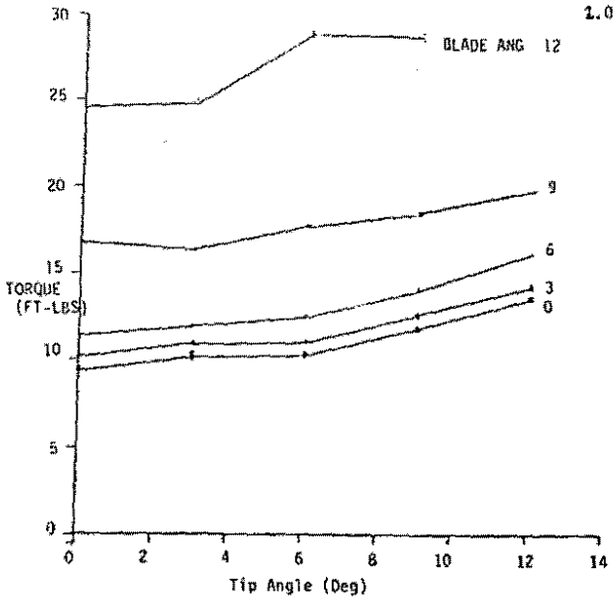

Figure 11. Torque VS. Tip Angle Constant RPM=643
Hover Test of H-Force Rotor
Data Averaged Over 10 REVS

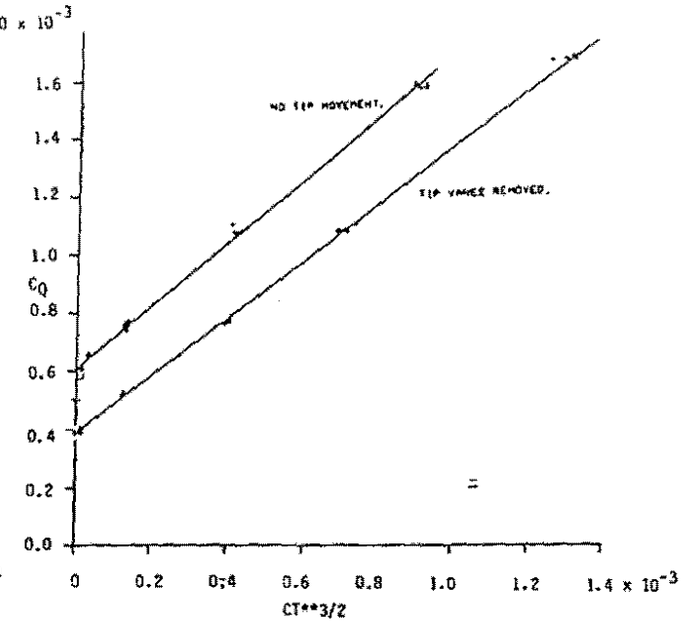

Figure 13. Comparison of Effect of Tip Vanes on the Torque Coefficient

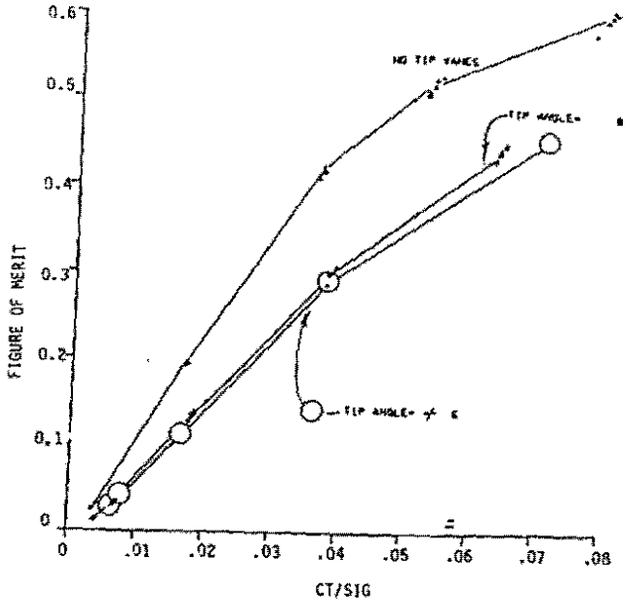

Figure 12. The Effect of Tip Vanes on Figure of Merit

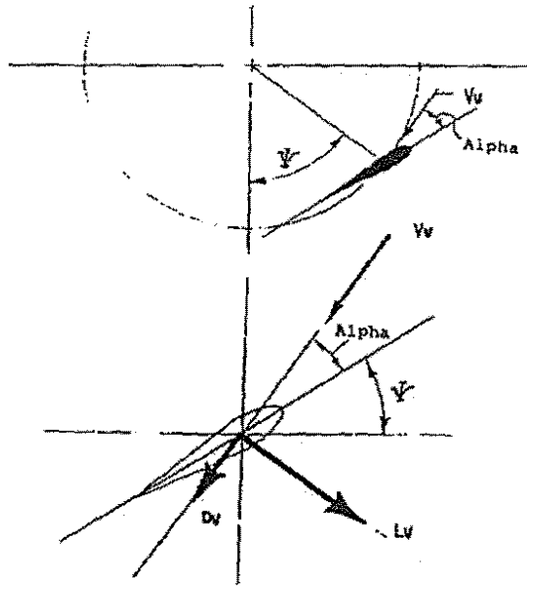

Figure 14. Definition of Tip Vane Variables.

APPENDIX I

List of Symbols

AR	= aspect ratio of vane
A	= rotor disk area
A_V	= vane
A_{wet}	= wetted area of vane
A_{ref}	= A_V
b	= number of blades
Cl	= a constant defined within equation
C_D	= total drag coefficient oif vane
C_{dp}	= profile drag coefficient of vane
C_d	= drag coefficient of vane-no oscillation
C_f	= skin friction coefficient
C_Q	= torque coefficient, = Q/ AV_TR
C_T	= Thrust coefficient
e	= span efficiency factor (Oswald factor)
F_x	= horizontal force in x direction
K	= a constant
N	= rotor speed, rpm
Q	= torque due to vane drag
R_V	= rotor radius to blade tip
R	= radius to vane pivot
V_T	= rotor tip speed
V_V	= vane tangential velocity
ρ	= density
Ω	= rotor rotational speed
η	= tip vane amplitude
Ψ	= azimuth position of vane/blade

Drag Coefficient Calculation

The effective drag-coefficient for the tip vane at zero blade angle and zero tip angle can be calculated as follows. The drag of the vane is given by

$$D_v = C_{Dv} \rho V_v^2 A_v / 2 \qquad (1)$$

Now $$Q_v = D_v R_v \cdot b \qquad (2)$$

and $$C_{Qv} = Q_v / \rho A V_T^2 R \qquad (3)$$

So $$= C_{Dv} \rho V_v^2 A_v R_v / 2 (\rho A V_T^2 R) \qquad (4)$$

$$V_T = \Omega R \ , \quad V_v = \Omega R_v$$

$$C_{Qv} = C_{Dv} (R_v/R)^3 (A_v/A) b/2 \qquad (5)$$

For the case shown in the $C_Q - C_T^{3/2}$ plot, A_V = .26 sq ft (.0242 sq m), R_V = 37.86 in, R = 40.0, N = 621 rpm, b = 3 blades, then C_{Q_V} = .003158 C_{Dv}. The increase in C_Q from the figure is .000605-.00039 = .00215. Thus C_{D_V} = 0.0227.

H-force Calculation

The geometry of the vane, the flow angles and the lift and drag forces are shown in figure 14.

To simplify the calculation the following assumptions were made.

1. Neglect the horizontal flow of air as it approaches the blade due to the radial inflow in hover. The hover contraction does not exist with zero blade angle. Assume that the velocity relative to the blade is always in the tangential direction with magnitude R_V.

2. Neglect the effect of any flow along the axis of the vane (2-D assumption)

3. Neglect the flow turning in the vicinity of the blade, and use the free stream velocity, V_v, as a reference direction for th lift and drag of the tip vane. In this case the lift will always be acting toward the center of rotation or outward in the radial direction. The drag will always act in the tangential direction.

The force in the x direction becomes:

$$F_X = L \sin\Psi - D \cos\Psi \qquad 6$$

The vane lift is $$L = C_L \rho V_v^2 A_v^2/2 \qquad 7$$

and $$C_{Lv} = a\alpha \qquad 8$$

$$a = d C_L/d\alpha = a_0/(1 + a_0/\pi AR) \qquad 9$$

and $$\alpha = \eta \sin\Psi \qquad 10$$

The vane total drag is: $$D_v = C_D \rho V_v^2 A_v/2 \qquad 11$$

and $$C_D = C_{Dp} + C_L^2 (\pi e AR)^{-1} \qquad 12$$

C_{dp} can be calculated from $$C_{dp} = K C_f A_{wet}/A_{ref} \qquad 13.$$

$$K = 1.35$$

Note $A_{wet}/A_{ref} \cong 2$

Substitute equations 9 and 10 into equation 8, then substitute equation 13 into 12 for C_D. Next substitute the equation 8 obtained into equation 7 for lift and equation 11 for drag. One obtains upon substitution into equation 6 for F_X

$$F_x(\Psi) = C_1 \eta (\sin\Psi)^2 - C_2 \cos\Psi - C_3 \eta^2 \sin^2\Psi \cos\Psi \qquad 14$$

The average value of the force can be obtained by solving for the mean value of F_X

$$\bar{F}_x = \frac{1}{2\pi} \int_0^{2\pi} F_x(\Psi)\, d\Psi \qquad 15$$

which becomes $$\bar{F}_x = C_1 \eta/2 \qquad 16$$

since upon integration the drag terms drop out.

For the example case with:

AR = 1 assuming no end plate effect of blade, η = 9°, ρ = 0.00234 slugs/ft^3, e = .93, N = 621 rpm, V_v = 205.2 ft/sec, A_v = 0.26 sq. ft., 90 = 5.75 then C_{Dp} = 0.016, a = 2.03 and the side force F_{x_b} = 1.98 lb per blade. The total side force is F_x = 5.94 lb. per blade.

This result is close to the value of 5.84 measured at zero pitch angle and a vane amplitude of 9°. Thus it appears that little end plate effect from the rotor blades is achieved.

Reference:

Shevell, R. S., Fundamentals of Flight, Prentice-Hall Inc., Englewood Cliffs, New Jersey, pages 145-183, 1983

APPENDIX II

Revised Instrumentation System

In order to be able to determine if there was an interaction between any lift changes due to vane motion and the side force measurements, modifications were made to the test stand instrumentation. An added set of flexures with gages was installed at the base of the mast and a revised data system was incorporated. A very brief description of these changes will be presented here.

Transducers

At the base of the mast, the rubber support diaphragm was replaced with another set of flexures. These were arranged at 90 degrees and were equipped with 350 Ohm strain gages. The entire mast was now suspended in flexures, so arranged that the forces in two planes located 30 in. (0.76 m) apart could be measured. By determining the X and Y forces in each of these planes it would then be possible to evaluate both the thrust and the moments generated by the action of the tip vanes as well as the azimuth of the peak force. The strain gages were connected to revised carrier amplifiers, solid state units that are expected to have less drift.

The data system used in the tests described in the body of the paper utilized an interactive system with the VAX 750 computer. The revised system utilized a local data acquisition system based upon a Wavetek 6000 data system. The data system acquires the data, stores it on a separate floppy disk for each case, processes it, and allows plots of the data to be made. The calibration, crosstalk matrix and data reduction system is essentially a modification of the older system.

Initial checkout runs of the new system have been made with the rotor and tip vanes activated. As of the time of this presentation, no data have been taken for record, but some indications exist that some moment may be generated due to tip vane motion.